Probing Field-Induced Tissue Polarization Using Transillumination Fluorescent Imaging

Bryan J. Caldwell,[†*] Marcel Wellner,[†‡] Bogdan G. Mitrea,[†] Arkady M. Pertsov,[†] and Christian W. Zemlin[†]
[†]Department of Pharmacology, State University of New York Upstate Medical University, Syracuse, New York; and [‡]Physics Department, Syracuse University, Syracuse, New York

ABSTRACT Despite major successes of biophysical theories in predicting the effects of electrical shocks within the heart, recent optical mapping studies have revealed two major discrepancies between theory and experiment: 1), the presence of negative bulk polarization recorded during strong shocks; and 2), the unexpectedly small surface polarization under shock electrodes. There is little consensus as to whether these differences result from deficiencies of experimental techniques, artifacts of tissue damage, or deficiencies of existing theories. Here, we take advantage of recently developed near-infrared voltage-sensitive dyes and transillumination optical imaging to perform, for the first time that we know of, noninvasive probing of field effects deep inside the intact ventricular wall. This technique removes some of the limitations encountered in previous experimental studies. We explicitly demonstrate that deep inside intact myocardial tissue preparations, strong electrical shocks do produce considerable negative bulk polarization previously inferred from surface recordings. We also demonstrate that near-threshold diastolic field stimulation produces activation of deep myocardial layers 2–6 mm away from the cathodal surface, contrary to theory. Using bidomain simulations we explore factors that may improve the agreement between theory and experiment. We show that the inclusion of negative asymmetric current can qualitatively explain negative bulk polarization in a discontinuous bidomain model.

INTRODUCTION

The effects of electrical fields on tissue have been attracting significant theoretical and experimental interest due to their wide-ranging applications. The most important and best studied application is defibrillation, where strong field shocks restore normal electrical activity and synchronized contractions in a fibrillating heart, enabling resuscitation of patients from sudden cardiac death. More recent applications use strong fields as a tool to deliver genetic material into cells (1,2) or for the targeted treatment of cancerous tissues (3,4).

Sophisticated biophysical theories have been developed that predict the distribution of the transmembrane and extracellular potentials inside the heart during electrical shocks. Major successes were the prediction of the dog-bone-shaped polarization in anisotropic myocardial tissue (5–7), the formation of quatrefoil reentry (8), and qualitative patterns of surface polarization during defibrillation shocks in the whole heart (9). However, recent optical imaging studies utilizing voltage-sensitive dyes have revealed several major discrepancies between theory and experiment that cannot readily be resolved.

One of these discrepancies is the presence of negative bulk polarization recorded during strong shocks (10) despite theoretical prediction of near-zero bulk polarization. A second discrepancy is the unexpectedly low degree of surface polarization (11) under the shock electrodes. The depth-averaging effect of optical mapping techniques (12) was shown to mask the degree of surface polarization. However, the masking effect cannot explain recently reported activation patterns during near-threshold diastolic field stimulation (13). Rather than emerging at the cathodal surface, where the magnitude of depolarization should be maximal (11,14–18), the early activation consistently occurs away from the cathode (12,13). This leads to the paradoxical conclusion that surface polarization during field stimulation may be less than intramural polarization.

The major obstacle to resolving these discrepancies was the lack of adequate techniques for assessing intramural polarization, or so-called virtual electrodes. Until recently, the degree of intramural polarization was assessed using measurements from the epicardial surface (19) or, more often, from the transmural cut edge of wedge preparations (10). Limitations of these approaches, in particular, unavoidable tissue damage characteristic of the cut-edge approach, have been a source of concern and controversy in the interpretation of experimental data (20).

The goal of this study is to explore noninvasively the effects of electrical fields deep inside the ventricular wall. To achieve this goal, we take advantage of near-infrared voltage-sensitive dyes (21) and transillumination imaging techniques (22,23) recently developed in our laboratory. Here, we carry out the first, to our knowledge, noninvasive measurements, of intramural bulk polarization during strong and weak electrical shocks. We also use the new technique to track early intramural activation during near-threshold diastolic field pacing. Finally, we use computer modeling to explore the possibility of reconciling current models with experimental observations.

Submitted December 23, 2009, and accepted for publication July 28, 2010.

*Correspondence: caldwelb@upstate.edu

Editor: Randall L. Rasmusson.

0006-3495/10/10/2058/9 $2.00

doi: 10.1016/j.bpj.2010.07.057

METHODS

Right ventricle slab preparation

All experimental protocols conformed to institutional and National Institutes of Health guidelines. Pigs of either sex (12–30 kg, $n = 4$) were intravenously anesthetized with sodium pentobarbital (35 mg/kg) and heparinized (500 IU). The heart was rapidly removed and chilled with 4°C cardioplegic solution. The right ventricle (RV) was quickly excised and the right coronary artery cannulated. Nonperfused tissue was removed, and the preparation was stretched on a plastic frame and mounted in a glass perfusion chamber. Preparations were perfused and superfused with warm (37°C) oxygenated Tyrode solution with 0.04 g/L albumin at a constant pressure of 80 mm Hg. After 30 min equilibration, 10–15 mmol/L of 2,3,-butanedione monoxime was added to extinguish contractions, and the preparation was stained with the near-infrared dye DI-4-ANBDQBS (40 μM).

The preparation was continually paced at 508-ms base cycle length from two 50 × 50-mm silver mesh electrodes (6 × 12 mm spacing) oriented parallel to the epi- and endocardial surfaces. The field electrodes were placed 32 mm apart and ~11 mm from the respective surfaces. This insured that the electric field was near uniform across the surface (variation of <10% measured in the bath). The amplitude was set at 2× threshold (1.2–1.8 V/cm, 5 ms). This was sufficient to provide near-simultaneous transmural activation and uniform phase distribution during a 10-ms shock applied 50 ms after the pacing stimulus. Shock strength was monitored in the tissue using two resin plunge needles with two bipolar electrodes (0.5 mm spacing). For near-threshold diastolic field pacing, the field amplitude was reduced to within 5–10% of the lowest voltage (0.6–1.1 V/cm, 5 ms) that sustained capture.

Alternating transillumination optical mapping

Fig. 1 shows the optical imaging system. Each surface of the preparation was alternately illuminated (compare Fig. 1, *A* and *B*) with one of two 600-mW, 660-nm lasers (Shanghai Dream Laser Technology, Shanghai, China). The laser beams were expanded by a holographic diffuser and directed onto the heart surface by a long-pass dichroic mirror (680DCLP, Chroma Technology, Rockingham, VT). Fluorescence images of the same (30 × 30 mm) area were simultaneously recorded from opposite sides of the preparation with two CCD cameras (Lil'Joe, Scimeasure Analytical Systems, Decatur, GA) at 80 × 80-pixel, 2-kHz, 14-bit resolution. The fluorescent light was isolated using 715-nm interference filters (Chroma Technology).

For each shock strength and field orientation, four movies (Fig. 1, PP, PN, NP, and NN) were recorded. The first letter refers to the position of the light source and the second to the position of the camera with respect to the ePicardium (P) and eNdocardium (N). The PP and PN movies were recorded when the light was directed to the epicardial (P) surface so that charge-coupled device camera CCD-1 recorded epifluorescence from the epicardium and CCD-2 simultaneously recorded transillumination from the endocardium (Fig. 1 *A*). When the excitation light was switched to the endocardial (N) surface (Fig. 1 *B*) and the shock was repeated, CCD-1 recorded transillumination from the epicardium (NP) and CCD-2 recorded epifluorescence from the endocardium (NN).

PP, PN, NP, and NN images contain different contributions from the layers across the ventricular wall, as quantified by the weighting functions presented in Fig. 2 (see Derivation in the Supporting Material). The weighting functions for the epifluorescence images PP and NN are largest in the 2 mm below the surface (~70% cumulative weight). In contrast, the transillumination images NP and PN are largest in the deep intramural layers (2–6 mm, ~70% cumulative weight). The NP and PN weighting functions have similar shape, but the epicardial subsurface layers (0–1 mm) contribute substantially more to NP than to PN, whereas the deeper layers (1–4 mm) contribute up to 15% more to PN than to NP. On the endocardial side, the roles are reversed. Note that the weighting functions in Fig. 2 describe planar sources induced by a uniform field that changes only transmurally (they are 1D weighting functions). For point sources of excitation (see Fig. 6), we use 3D weighting functions described elsewhere (23). We generally displayed the four images according to the depth at which the weighting function has its maximum; for 1D weighting functions, this is PP, PN, NP, NN, and for 3D weighting functions, it is PP, NP, PN, NN.

Temporal and spatial averaging filters (diameters 2.5 ms and 3.4 mm for plateau shock, 1.5 ms and 1.9 mm for diastolic field pacing) were applied to all frames. These filter parameters have been shown to improve signal/noise ratio with little effect on action potential (AP) morphology (24). Shock-induced transmembrane voltage (ΔV_m) (Fig. 3 *A*) was estimated at shock end by subtracting the ensemble-averaged AP (12–16 beats) generated by field pacing in the absence of the shock (Fig. 3 *B*). If ΔV_m was less than the mean peak noise amplitude, it was set to zero. Activation time was estimated from dF/dt_{max} of the AP upstroke, and referenced to the stimulus onset.

Computer simulations

A bidomain model was used to simulate electrical activity in response to uniform field stimulation inside an 8-mm slab of myocardial tissue. To reduce computation to 1D, fibers were assumed parallel to the epicardium,

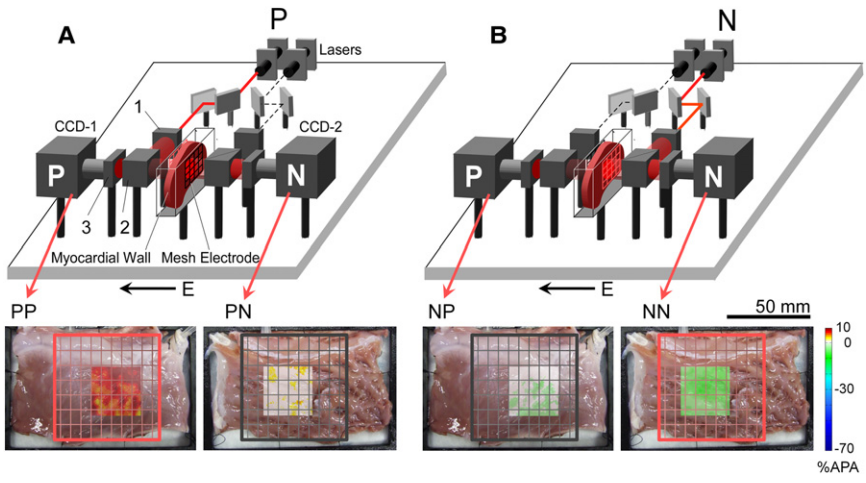

FIGURE 1 Alternating transillumination mapping system. The RV preparation is mounted in a glass perfusion chamber between two CCD cameras. For each shock strength and field orientation, four movies (PP, PN, NP, and NN) were recorded. The first letter refers to the position of the light source and the second letter to the position of the camera with respect to the ePicardium (P) and eNdocardium (N). (*A*) Light from a single 600-mW, 660-nm laser is expanded by a holographic diffuser (*1*) and directed to the epicardial surface (P) via a dichroic mirror (*2*). Fluorescent emission is long-pass filtered at 715 nm (*3*) and recorded by CCD-1 as epifluorescence (PP) and by CCD-2, from the endocardial surface (N), as transillumination (PN). (*B*) Laser light is now directed toward the endocardial surface (N), where CCD-1 records transillumination (NP) and CCD-2 records epifluorescence (NN). Field electrodes are shown superimposed on the tissue surfaces at the bottom of the figure, red corresponding to epifluorescence and black to transillumination. (*Insets*) Camera views showing ΔV_m for a field (E) oriented from N to P.

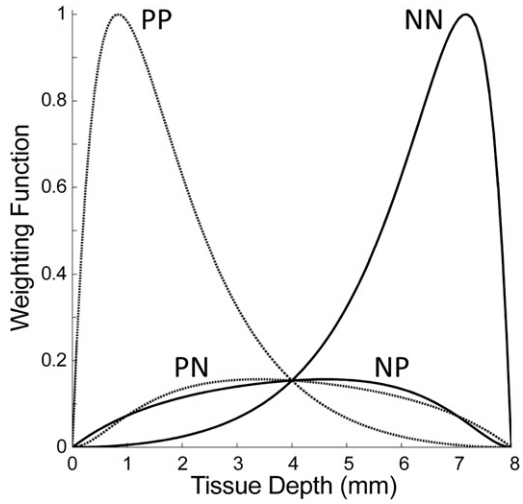

FIGURE 2 Weighting functions for epifluorescence and transillumination images. Attenuation lengths (mm) are $\alpha = 2.56$ for diffuse photons, $b = a/4$ for ballistic photons, and $f = 3.3$ for near-infrared dye emission. PP, PN, NP, and NN are defined in Fig. 1 legend.

so there is no epiparallel component of the electrical field. Intracellular transmural conductivity (gi) and interstitial transversal conductivity (ge) were set so that the ge/gi ratio is 2.5, as is generally accepted (25,26),

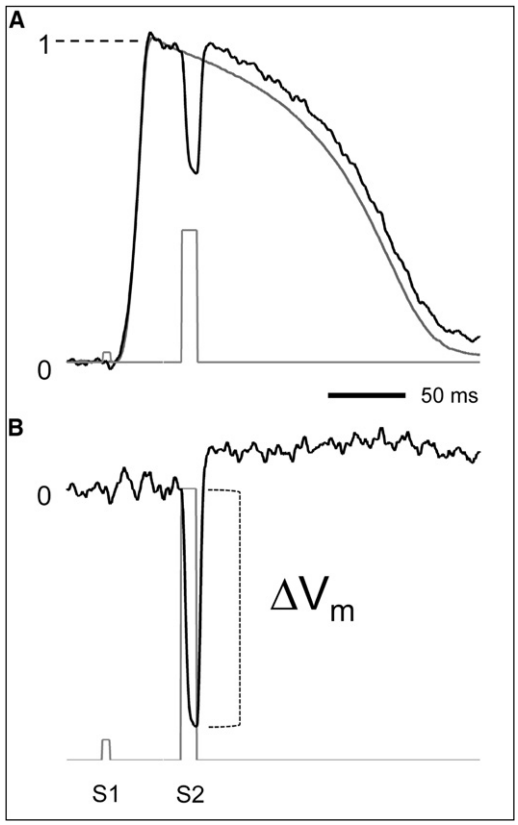

FIGURE 3 Measurement of ΔV_m. (*A*) A typical ensemble-averaged optical AP is overlain with the AP showing the response to strong shock during the plateau phase. The AP amplitude (APA) is normalized. S1 pacing and S2 shock markers are depicted at base line. (*B*) Result of subtracting the APs in *A*. ΔV_m is measured at S2 end and presented as a percentage of the APA (% APA).

and the transmural conduction velocity was 34 cm/s (27). This led to ge = 0.8 S/m and gi = 0.32 S/m. To incorporate the layered structure of the myocardium, which is oriented at a mean angle of −25° to the transmural z axis (27,28), intracellular coupling was reduced to 0.1 gi randomly every 2–8 cells, corresponding to layer thicknesses of 30–120 μm. These reductions of gi reflect the discontinuity of the intracellular domain in the transmural direction. The surface/volume ratio was set to 2700/cm, corresponding to a cylindrical cell geometry with a radius of 7.5 μm. Transmembrane currents were computed using the Luo-Rudy II dynamic model (29). In some simulations, the model was augmented for high field strengths by incorporating an additional outward current (I_a) activated at large depolarizing voltages (30).

We used a time step of 1 μs during shocks and 5 μs for propagation, and a space step of 17 μm. An AP was initiated by 5-ms stimulus current to all model cells simultaneously, and a 10-ms-duration 30 V/cm shock was applied after 50 ms during the plateau phase. Near-threshold diastolic field pacing was evaluated by varying the amplitude of a 5-ms-duration stimulus from 0.9 to 6.3 V/cm.

To model the effect of a shock on the optical signal, model results were convolved with the optical weighting functions shown in Fig. 2.

RESULTS

Plateau-phase shocks

The experiments were conducted for two shock strengths: weak shocks of ~3 V/cm and strong shocks of ~30 V/cm. To achieve uniformity of AP phase throughout the wall during the plateau shock, we generated a uniform field pacing stimulus at two times threshold (1.2–1.8 V/cm). Fig. 4 *A* shows typical activation maps of the epicardial (PP), endocardial (NN), and transmural (PN and NP) layers after that field stimulus. Although the amplitude of the stimulus is relatively small (1.5 V/cm), the spatial dispersion of

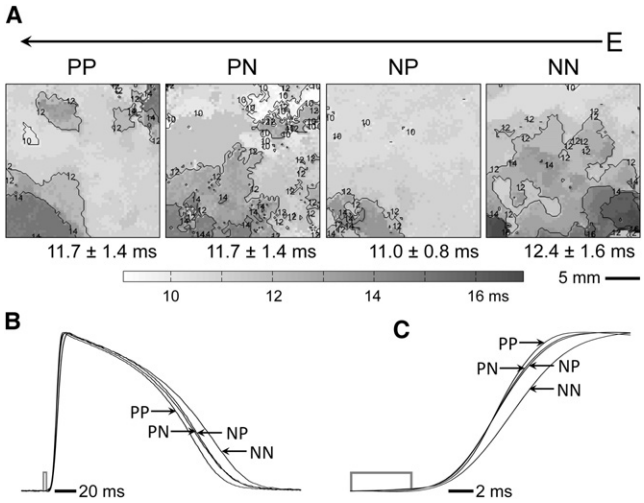

FIGURE 4 Activation during uniform field pacing at twice the excitation threshold (1.5 V/cm). (*A*) Activation maps superimposed with isochrones at 2-ms intervals. Mean activation time and SD is displayed below the respective map. The field direction (E) is indicated at the top of the figure. PP, PN, NP, NN are defined in Fig. 1 legend. (*B*) Normalized AP averaged over all pixels from each optical movie are superimposed. (*C*) Close-up of the AP upstrokes from *B*. The stimulus markers for both *B* and *C* are shown at base line.

activation time in any image had a standard deviation of <1.6 ms. This means that all cells across the entire wall are practically in the same state at the time of the plateau shock. This is further highlighted in Fig. 4, *B* and *C*, which shows the average APs from all pixels in each layer, with the full APs and a close-up of the upstroke, respectively. In each panel, it is clear that activation is near-simultaneous in all layers, with a slight delay (~2 ms) at the endocardial surface (NN). This is a significant improvement over commonly used point-stimulus pacing (10).

The results for weak shock strengths (3.6 V/cm) are illustrated in Fig. 5 *A*. At the cathode (NN), polarization is uniformly positive (yellow to red, 3.1 ± 0.7% AP amplitude (APA)), whereas at the anode (PP) it is uniformly negative (green, −5.3 ± 1.2% APA). The shock response in PN and NP transillumination images, representing bulk polarization in deep myocardial layers, is near zero (predominantly white, −1.0 ± 1.2 and 0.1 ± 0.4% APA, respectively). The APs beneath the color panels are the average APs from all pixels in each panel. They highlight the very weak response to the shock both at the surfaces and in intramural layers. Our analysis shows that even taking into account depth-averaging effects of optical recordings, the observed surface polarization is still much smaller than can be explained by existing theories.

For strong shocks (35.1 V/cm) (Fig. 5 *B*), polarization was strongly negative everywhere in epifluorescence (PP and NN) and transillumination (PN and NP) images and it was maximal at the anode (PP, deep blue, −64.6 ± 5.1% APA). We also observed negative polarization at the cathode (NN, deep green to blue, −30.5 ± 5.7% APA). Unlike weak shocks, strong shocks produced significant negative bulk polarization, as seen in the transillumination images (NP and PN, blue, −43.7 ± 1.9 and −46.5 ± 2.4% APA, respectively). These observations are consistent with early observations by the Fast group (10) but contradict conventional theory (see Bidomain simulations, below, and Discussion).

The effects of both weak and strong shocks under the anode and cathode are reproduced after the reversal of shock polarity (see Fig. S5 in the Supporting Material). Shock data are summarized in Table 1. Independent of shock polarity, in all but one recording, the amplitude of response was larger at the epicardial than at the endocardial surface (see Table S2).

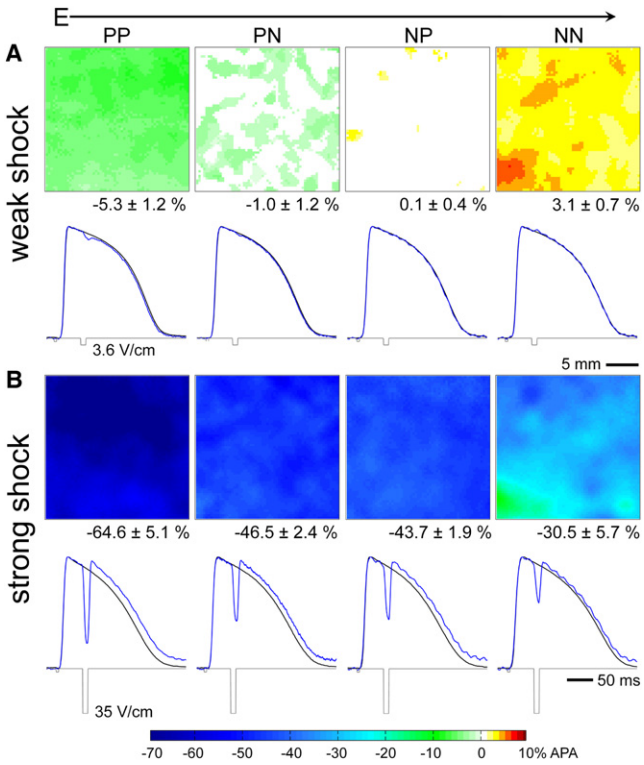

FIGURE 5 ΔV_m during weak shock (3.6 V/cm) (*A*) and strong shock (35.1 V/cm) (*B*) applied during the plateau phase of optical APs generated by uniform field pacing (see Fig. 4). ΔV_m is displayed as % APA in the color maps, with the corresponding preshock (*black*), and during-shock (*blue*) normalized AP averaged over all pixels displayed below. S1 pacing and S2 shock markers are depicted at base line. ΔV_m, expressed as mean ± SD, is shown below each map.

Near-threshold diastolic shocks

According to classical bidomain theories, a diastolic field shock just above the excitation threshold should activate only a thin layer of tissue under the cathode. This activated layer should give rise to an activation wave propagating transmurally from cathode to anode. However, this is not what we observe experimentally. Analysis of our transillumination data shows that diastolic shocks <10% above the excitation threshold induce activation not only at the cathodal surface but also at the anodal surface and within the wall.

An example of such multisite activation produced by a 0.9 V/cm, 5-ms diastolic shock is shown in Fig. 6. Fig. 6 *A* shows the PP, PN, NP, and NN snapshots 17 ms after the onset of shock. Small circles show the *x*,*y* coordinates of the centers of early activated regions (labeled 1–3). The time-dependent signals in the respective locations are shown below the snapshots. The analysis of these signals implies that regions 1 and 2 are located near the endocardium (anode), whereas region 3 spans almost the entire ventricular wall.

Indeed, at region 1, the NN signal appears first, 1–2 ms after the end of the shock. It is followed 4 ms later by the rise in PN and NP and 10 ms later by the PP signal. This indicates that the excitation starts near the endocardium (anode) and subsequently propagates toward the epicardium. Region 2 is activated a little later than region 1 (5 ms after the shock end). Again, as in region 1, the NN signal appears first, which indicates that the activation source is located closer to the endocardium. Unlike in region 1, however, the increase in the NN signal is almost

TABLE 1 Mean % APA across all experiments for weak and strong shocks

Mean V/cm	PP	PN	NP	NN	Field polarity
2.6 ± 0.4	5.8 ± 2.5	0.8 ± 1.3	−0.5 ± 1.1	−3.8 ± 1.4	Cathode P
2.8 ± 0.7	−6.1 ± 1.7	−1.0 ± 1.5	0.2 ± 0.7	3.1 ± 0.7	Anode P
34.2 ± 0.8	−24.2 ± 7.1	−33.7 ± 3.6	−35.4 ± 4.5	−42.3 ± 4.6	Cathode P
34.0 ± 1.2	−56.8 ± 7.3	−42.2 ± 4.7	−39.0 ± 4.2	−25.2 ± 6.6	Anode P

% APA is expressed as the mean ± SD for all shocks. Weak shocks were 2–4 V/cm and strong shocks were 32–35 V/cm.

immediately followed by an increase in PP, PN, and NP signals, suggesting that region 2 spans almost the entire thickness of the wall. Region 3 is activated almost simultaneously with region 2. Similar to region 2, it is also very large, as indicated by almost simultaneous intramural and surface activation.

Note that the sites of early activation feature a slow rising phase (foot) that starts immediately after the stimulus. The foot of the optical AP is >5 ms, which is very slow compared to what would be observed in electrical recordings. This is a consequence of spatial integration resulting from light-scattering and depth-averaging effects intrinsic to optical recordings (31) and most likely reflects an incremental increase in the volume of tissue activated during the weak shock.

In Fig. 6 *B*, we present conventional isochronal maps derived from PP, PN, NP, and NN recordings in the same experiment. The activation time was determined from the time of dF/dt_{max}. In all four maps, the earliest activation contours are 23 ms (18 ms after shock end). This clearly shows that weak shocks do not produce propagation from cathodal to anodal surface as predicted by theory.

Similar multisite activation with early activation sites scattered throughout the ventricular wall was observed in all experiments. It is interesting that reversal of field polarity did not always preserve the location of the early activation sites. Fig. S6 shows the effect of the reversal of field polarity in the experiment illustrated in Fig. 6. It also shows multiple activation sites spread across the entire thickness of the ventricular wall.

Computer simulations

To compare our experimental observations with theoretical predictions, we simulated optical action potentials and shock responses for all types (PP, PN, NP, and NN) of

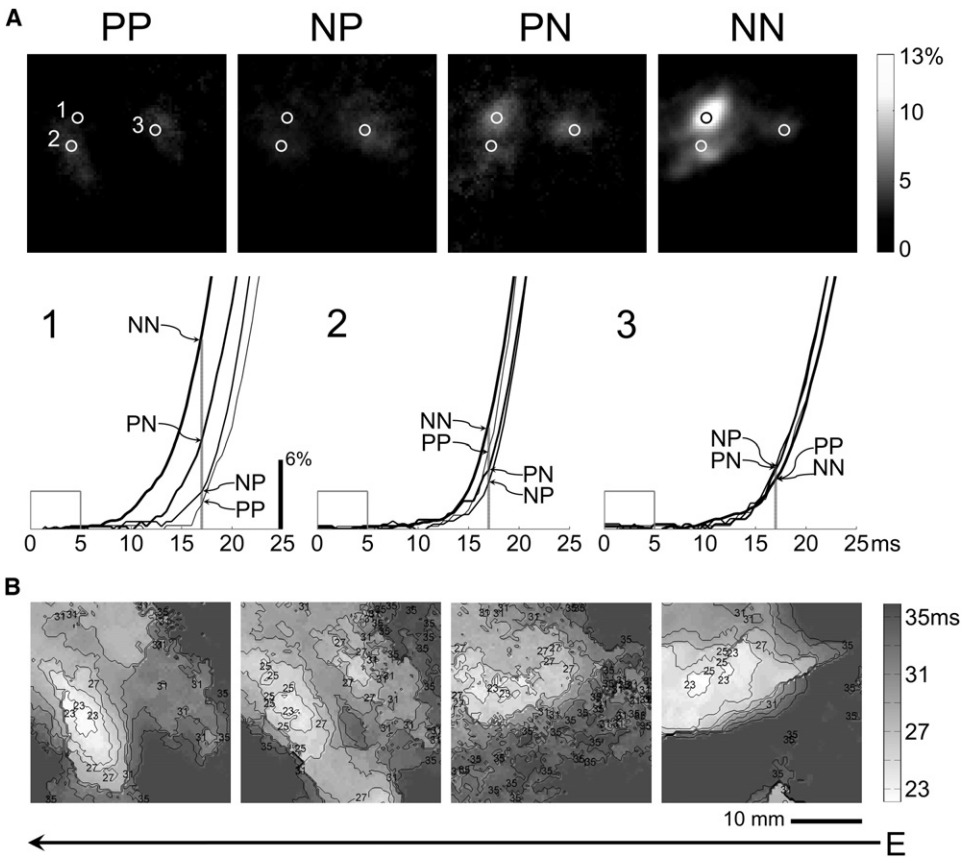

FIGURE 6 Intramural activation initiated by near-threshold diastolic field pacing (0.9 V/cm). The cathode is at the epicardial surface (PP). (*A*) Normalized AP 17 ms after stimulus onset (see color bar at right). The three earliest activating regions (*1–3*) correspond to the close-up of AP upstrokes in insets 1–3. Upstroke line thickness corresponds to the optical plane in *A*, with PP represented by the thinnest line, NP and PN by lines of intermediate thickness, and NN by the thickest line. The gray vertical line marks the 17-ms interval shown in *A*. The duration of the stimulus is shown at the beginning of the plots. (*B*) Activation contour maps are colored according to the color bar at right, with 2-ms contour lines superimposed.

recordings and experimental protocols. We calculated the transmural distributions of V_m using a bidomain model with Luo-Rudy (LRd) membrane kinetics. To simulate optical responses, we convolved these voltage distributions with the optical weighting functions derived from the realistic light transport model of myocardial tissue (see the Supporting Material).

Fig. 7 shows simulated optical responses to weak (3 V/cm) and strong (30 V/cm) shocks applied during the plateau phase of the AP for standard and augmented models. Fig. 7 *A* shows the simulations utilizing the standard LRd model. Fig. 7 *B* shows the results for the augmented LRd model with added asymmetric negative current (I_a), activated at high transmembrane voltages (see Methods).

For weak shocks (3 V/cm), the simulated responses are practically identical for both models (compare Fig. 7, *A* and *B*, *upper rows*). The predicted surface polarization is positive under the cathode and negative under the anode, which is consistent with our experimental observations (see Fig. 5). It should be noted, however, that the amplitudes of the simulated surface responses (PP = −9.6 and NN = 11.1% APA) are approximately two to three times larger than those recorded experimentally (PP = −5.8 and NN = 3.1% APA). This discrepancy is not likely to be rooted in the optical model, but rather reflects a fundamental problem of existing electrical models (see Discussion).

For strong shocks (30 V/cm), the predictions of the standard and augmented models diverge significantly (Fig. 7 *A*). The standard LRd model predicts significant depolarization (129.4% APA) at NN under the cathode, whereas experimentally we observe hyperpolarization of −30.5% APA (Fig. 5 *B*). The model also fails to predict the correct sign of the optical responses in the intramural PN and NP layers as well. Finally, the biphasic responses apparent in simulated PP, PN, NP, and NN recordings are largely absent in real experimental data.

Using the augmented model (Fig. 7 *B*) considerably improves the agreement between theory and experiment for strong shocks. The augmented model not only accurately predicts the sign of responses in all recording modes (−50.4, −20.1, −22.2, −35.1% APA for PP, PN, NP, and NN, respectively), but also more accurately reproduces their magnitude and kinetics, bringing the model predictions closer to experimental observations (compare with Fig. 5 *B*).

Simulation results of diastolic near-threshold field stimulation are illustrated in Fig. 8. Fig. 8 *A* shows time-space plots indicating the changes in spatial distribution of the transmembrane voltage across the myocardial wall during and after the shock for four different field strengths. Fig. 8 *A* (*left*) shows the time-space plot for the threshold shock (0.9 V/cm). The color scale (*lower right*) indicates the transmembrane potential. The excitation starts near the depolarized cathodal surface (*white arrows*) and propagates toward the opposite surface. The characteristic alternating blue (hyperpolarization) and red (depolarization) stripes, visible on each plot between 1 and 6 ms during the stimulus, represent intramural virtual electrodes, also known as a sawtooth pattern. In our model, these electrodes represent boundaries between myocardial bundles. The same pattern of excitation with the origin at the cathodal surface is preserved as the shock amplitude increases up to 4.5 V/cm (five thresholds).

The characteristics of the response change when the shock strength reaches 6 V/cm. At this voltage, in addition to the surface source of excitation we see the emergence of an intramural excitation source. Indeed, one of the intramural virtual electrodes located >6 mm away from the cathodal surface (*gray arrow*) gives rise to an expanding excitation wave. At the end of the 4.5-V/cm stimulus, one can also see a local transient depolarization at the same site, although the depolarization is too weak to initiate a propagating wave. The position of the secondary excitation site is random and is determined by the initial distribution of heterogeneities (in our case, boundaries between myocardial bundles). Further increase in shock strength from 6 V/cm to 7.5 V/cm produces multiple excitation centers all the way across the thickness of the myocardial wall, causing almost simultaneous ventricular excitation.

Fig. 8 *B* shows the PP, PN, NP, and NN simulated optical responses for all field strengths. The left three panels, corresponding to lower shock strengths, show that the cathodal upstroke occurs first, the intramural upstroke after a delay, and the anodal upstroke after an even longer delay. This characteristic sequence reflects the intramural activation sequence shown in Fig. 8 *A*. Our experimental recordings, however, do not follow this sequence. For both weak shocks

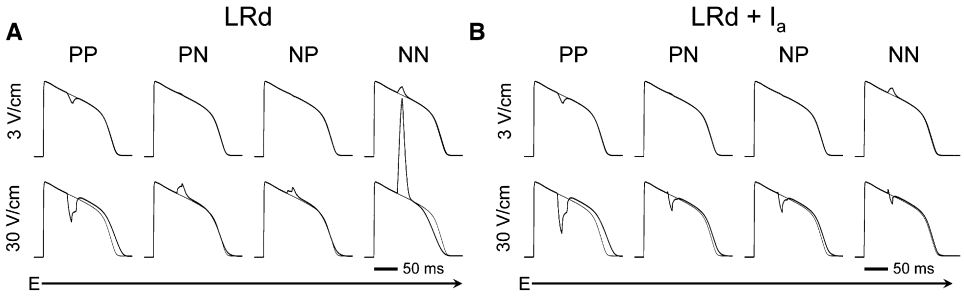

FIGURE 7 Simulated optical APs of shock-induced V_m during the plateau phase for different electrophysiological models. The shock-affected AP (*thick line*) is superimposed on the standard LRd AP (*thin line*). The effects of a weak (3 V/cm) and a strong shock (30 V/cm) are shown for the standard LRd II dynamical model (*LRd*) (*A*), and the modified model with I_a (*B*). The cathode is at the endocardial surface (NN).

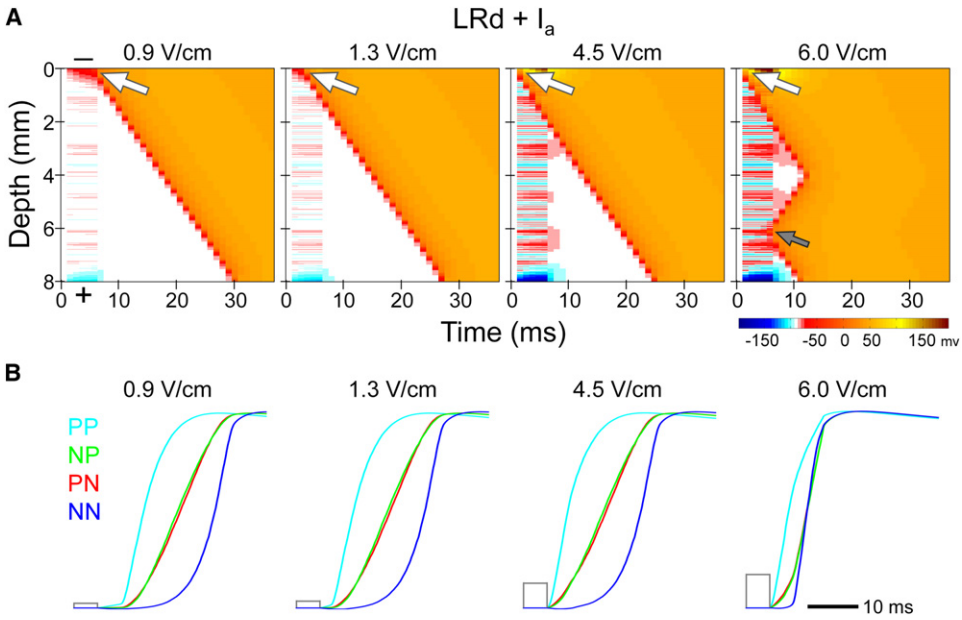

FIGURE 8 Simulated V_m for near-threshold to six-times-threshold diastolic shocks (0.9–6.0 V/cm). (*A*) Time-space plot of Vm across the myocardial wall. The standard LRd model was modified with I_a. The shock duration is apparent from 1 to 6 ms as an alternating polarized band. Field polarity for each plot is indicated above and below the band in the left-most plot. Resting membrane potential (~−89 mV) is colored white with depolarization red and hyperpolarization blue (see color bar at lower right). Surface activation (*white arrow*) occurs at 0.9 V/cm and intramural activation (*gray arrow*) at 6.0 V/cm. (*B*) Close-up of the upstroke of simulated optical APs of the time-space plots above. Colors are defined in panel *B*.

(Fig. 4 *C*) and near-threshold stimulation (Fig. 6 and Fig. S6), the upstroke sequences are more similar to multisite responses, which occur in the model at much larger (6.0 V/cm) field strengths.

DISCUSSION

This study explores the effects of electrical fields deep inside the ventricular wall using recently developed noninvasive transillumination imaging techniques (22,23) and near-infrared voltage-sensitive dyes (21). With this what we believe is a novel approach, we obtain a direct view of the effects of electrical fields on deep intramural myocardial tissue not previously available, to our knowledge.

Negative bulk polarization

As mentioned in the introduction, one of the discrepancies of field-induced myocardial tissue polarization is negative bulk polarization spanning almost the entire thickness of the myocardial wall and changing sign only at the very vicinity of the cathodal surfaces. This effect has been observed during strong shocks (>25 V/cm) applied during the plateau phase of the AP (10,19,32–34) and is attributed to some asymmetric negative current I_a, which shifts the inherent positive bias in the LRd model to a negative bias during such shocks (35). The existence of I_a is inferred from fluorescence imaging experiments, but its ionic nature remains poorly understood. An experimental study by Cheek et al. (36) suggests that I_a may flow through the L-type Ca^{2+} channel. However, the measurements of I_a have yet to be corroborated by direct voltage-clamp experiments.

In previous simulations in continuous bidomain models (20,35), I_a did introduce a negative bias, but qualitative differences with experimental data remained. In particular, the simulations still predicted a positive shock-induced deflection in the cathodal epifluorescence signal. This led some researchers to question the validity of the experimentally observed negative bulk polarization (20). Their concern was that negative polarization in the cathodal epifluorescence signal might be the consequence of tissue damage inflicted by the cut-edge technique.

In this study, we use a different experimental approach, which enables us to determine bulk intramural polarization noninvasively. By using transillumination imaging techniques and near-infrared voltage-sensitive dyes, we assess the intramural polarization in intact cardiac tissue far from the boundaries, which eliminates possible effects of tissue damage. We show (see Fig. 5 and Fig. S5) that negative bulk polarization is equally strong in both transillumination images (NP and PN) that represent mid-myocardium. We also observe significant hyperpolarization under the cathodal surface. Our findings are consistent with earlier experimental reports and provide unequivocal evidence that negative bulk polarization is not an artifact of tissue damage.

Here, we demonstrate that negative bulk polarization can be largely reproduced computationally in a discontinuous rather than continuous bidomain model (see Fig. 7). Despite the presence of a negative bias produced by I_a, in continuous bidomain models (20,35), a substantial volume underneath the cathode is depolarized. In contrast, in the discontinuous model, I_a gives rise to negatively biased polarization patterns at every discontinuity, even in the direct vicinity of the cathode. As a result, we see negative polarization throughout the wall and achieve good agreement with our experiments.

Weak plateau-phase shocks

Our experiments show that weak 2- to 3-V/cm plateau-phase shocks produce very little bulk polarization, which is consistent with bidomain simulations. Indeed, simulated optical responses to weak shocks look very similar to real experimental recordings (compare Fig. 7 with Fig. 5).

It should be noted, however, that the amplitudes of simulated surface optical responses are 2–3 times larger than those recorded experimentally. Considering that our computational light transport model uses Dirichlet boundary conditions (see the Supporting Materials), and therefore has a tendency to underestimate the contribution of surface layers, the discrepancy between theory and experiments is likely to be even larger. This means that at weak shocks, the real field-induced surface polarization is significantly smaller than that predicted by theory. This conclusion is further corroborated by the results of near-threshold diastolic field stimulation (see next section).

Near-threshold diastolic shocks

Current bidomain models (11,14–18) predict that shock-induced surface potentials are much larger than intramural virtual electrode potentials and that during near-threshold diastolic field stimulation, activation originates in a thin layer under the cathode and then propagates toward the anode. In theory, the activation of intramural layers requires much larger field strengths that exceed several times the activation threshold (see Fig. 8).

In contrast, during near-threshold field stimulation, our experiments show, for the first time that we know of, the location of multisite activation patterns spanning the entire thickness of the wall. We show examples in which early activation occurs in deep myocardial layers (2–6 mm) far from the cathodal surface, as well as cases of anodal excitation. The cathodal surface is typically not activated directly, but significantly after the end of the shock. This finding has been reported previously from optical recordings taken only from the ventricular surface (12,13,33,37).

What kind of changes to current bidomain models are needed to reproduce these experimental results? Adding a current to continuous models that limits depolarization (e.g., I_a) is insufficient, because even in such an augmented model, surface polarization still exceeds intramural polarization (20,35). Since intramural activation results from discontinuities on different spatial scales, accurately incorporating such discontinuities appears to be the most promising approach. Indeed, bidomain models that carefully determine the extent of the intracellular domain reproduce some aspects of the tissue response to strong shocks (38). However, they still fail to reproduce intramural activation during weak shocks. Instead, they show that the surface activates first (17,18), with a significant gap between surface and intramural excitation thresholds. A recent study showed that intramural activation can be achieved for certain distributions of heterogeneities even for weak shocks (13), but the distributions used in this study were not based on experimental measurement, and it is unclear whether similar distributions underlie intramural activation in real tissue.

It remains to be seen whether intramural activation for near-threshold field stimulation can eventually be reproduced in a bidomain model that better captures tissue discontinuities. Another possibility is that the detailed cellular structure of cardiac tissue, which is not included in bidomain models, is crucial to correctly predict the shock response of tissue. In this case, new types of models would be needed to take our understanding of the effects of electrical fields on tissue to the next level (39,40).

SUPPORTING MATERIAL

Nine equations, references, a table, and two figures are available at http://www.biophysj.org/biophysj/supplemental/S0006-3495(10)00931-8.

Research in this article has been supported by R01 Grant 47268 from the National Institutes of Health and American Heart Association Grants 0830018N and 0815731D.

REFERENCES

1. Escoffre, J. M., D. S. Dean, …, C. Favard. 2007. Membrane perturbation by an external electric field: a mechanism to permit molecular uptake. *Eur. Biophys. J.* 36:973–983.
2. Beebe, S. J., J. White, …, K. H. Schoenbach. 2003. Diverse effects of nanosecond pulsed electric fields on cells and tissues. *DNA Cell Biol.* 22:785–796.
3. Nuccitelli, R., X. Chen, …, K. H. Schoenbach. 2009. A new pulsed electric field therapy for melanoma disrupts the tumor's blood supply and causes complete remission without recurrence. *Int. J. Cancer.* 125:438–445.
4. Esser, A. T., K. C. Smith, …, J. C. Weaver. 2007. Towards solid tumor treatment by irreversible electroporation: intrinsic redistribution of fields and currents in tissue. *Technol. Cancer Res. Treat.* 6:261–274.
5. Roth, B. J., and J. P. Wikswo, Jr. 1994. Electrical stimulation of cardiac tissue: a bidomain model with active membrane properties. *IEEE Trans. Biomed. Eng.* 41:232–240.
6. Wikswo, Jr., J. P., T. A. Wisialowski, …, D. M. Roden. 1991. Virtual cathode effects during stimulation of cardiac muscle. Two-dimensional in vivo experiments. *Circ. Res.* 68:513–530.
7. Sambelashvili, A. T., V. P. Nikolski, and I. R. Efimov. 2003. Nonlinear effects in subthreshold virtual electrode polarization. *Am. J. Physiol. Heart Circ. Physiol.* 284:H2368–H2374.
8. Lin, S. F., B. J. Roth, and J. P. Wikswo, Jr. 1999. Quatrefoil reentry in myocardium: an optical imaging study of the induction mechanism. *J. Cardiovasc. Electrophysiol.* 10:574–586.
9. Efimov, I. R., F. Aguel, …, N. Trayanova. 2000. Virtual electrode polarization in the far field: implications for external defibrillation. *Am. J. Physiol. Heart Circ. Physiol.* 279:H1055–H1070.
10. Fast, V. G., O. F. Sharifov, …, R. E. Ideker. 2002. Intramural virtual electrodes during defibrillation shocks in left ventricular wall assessed by optical mapping of membrane potential. *Circulation.* 106: 1007–1014.
11. Wikswo, Jr., J. P., S.-F. Lin, and R. A. Abbas. 1995. Virtual electrodes in cardiac tissue: a common mechanism for anodal and cathodal stimulation. *Biophys. J.* 69:2195–2210.

12. Sharifov, O. F., and V. G. Fast. 2006. Role of intramural virtual electrodes in shock-induced activation of left ventricle: optical measurements from the intact epicardial surface. *Heart Rhythm.* 3:1063–1073.

13. Zemlin, C. W., S. Mironov, and A. M. Pertsov. 2006. Near-threshold field stimulation: intramural versus surface activation. *Cardiovasc. Res.* 69:98–106.

14. Plonsey, R., and R. C. Barr. 1986. Effect of microscopic and macroscopic discontinuities on the response of cardiac tissue to defibrillating (stimulating) currents. *Med. Biol. Eng. Comput.* 24:130–136.

15. Fast, V. G., S. Rohr, …, A. G. Kléber. 1998. Activation of cardiac tissue by extracellular electrical shocks: formation of "secondary sources" at intercellular clefts in monolayers of cultured myocytes. *Circ. Res.* 82:375–385.

16. Trayanova, N., K. Skouibine, and F. Aguel. 1998. The role of cardiac tissue structure in defibrillation. *Chaos.* 8:221–233.

17. Fenton, F. H., S. Luther, …, R. F. Gilmour, Jr. 2009. Termination of atrial fibrillation using pulsed low-energy far-field stimulation. *Circulation.* 120:467–476.

18. Hooks, D. A., M. L. Trew, …, A. J. Pullan. 2006. Do intramural virtual electrodes facilitate successful defibrillation? Model-based analysis of experimental evidence. *J. Cardiovasc. Electrophysiol.* 17:305–311.

19. Sharifov, O. F., V. G. Fast, V. G. Fast…, 2004. Intramural virtual electrodes in ventricular wall: effects on epicardial polarizations. *Circulation.* 109:2349–2356.

20. Plank, G., A. Prassl, …, N. A. Trayanova. 2008. Evaluating intramural virtual electrodes in the myocardial wedge preparation: simulations of experimental conditions. *Biophys. J.* 94:1904–1915.

21. Matiukas, A., B. G. Mitrea, …, L. M. Loew. 2007. Near-infrared voltage-sensitive fluorescent dyes optimized for optical mapping in blood-perfused myocardium. *Heart Rhythm.* 4:1441–1451.

22. Baxter, W. T., S. F. Mironov, …, A. M. Pertsov. 2001. Visualizing excitation waves inside cardiac muscle using transillumination. *Biophys. J.* 80:516–530.

23. Mitrea, B. G., M. Wellner, and A. M. Pertsov. 2009. Monitoring intramyocardial reentry using alternating transillumination. *Conf. Proc. IEEE Eng. Med. Biol. Soc.* 2009:4194–4197.

24. Mironov, S. F., F. J. Vetter, and A. M. Pertsov. 2006. Fluorescence imaging of cardiac propagation: spectral properties and filtering of optical action potentials. *Am. J. Physiol. Heart Circ. Physiol.* 291: H327–H335.

25. Sepulveda, N. G., B. J. Roth, and J. P. Wikswo, Jr. 1989. Current injection into a two-dimensional anisotropic bidomain. *Biophys. J.* 55: 987–999.

26. Roth, B. J. 1991. Action potential propagation in a thick strand of cardiac muscle. *Circ. Res.* 68:162–173.

27. Caldwell, B. J., M. L. Trew, …, B. H. Smaill. 2009. Three distinct directions of intramural activation reveal nonuniform side-to-side electrical coupling of ventricular myocytes. *Circ. Arrhythm. Electrophysiol.* 2:433–440.

28. LeGrice, I. J., B. H. Smaill, …, P. J. Hunter. 1995. Laminar structure of the heart: ventricular myocyte arrangement and connective tissue architecture in the dog. *Am. J. Physiol.* 269:H571–H582.

29. Luo, C. H., and Y. Rudy. 1994. A dynamic model of the cardiac ventricular action potential. I. Simulations of ionic currents and concentration changes. *Circ. Res.* 74:1071–1096.

30. Cheng, D. K., L. Tung, and E. A. Sobie. 1999. Nonuniform responses of transmembrane potential during electric field stimulation of single cardiac cells. *Am. J. Physiol.* 277:H351–H362.

31. Hyatt, C. J., S. F. Mironov, …, A. M. Pertsov. 2005. Optical action potential upstroke morphology reveals near-surface transmural propagation direction. *Circ. Res.* 97:277–284.

32. Cheek, E. R., V. G. Fast, V. G. Fast…, 2004. Nonlinear changes of transmembrane potential during electrical shocks: role of membrane electroporation. *Circ. Res.* 94:208–214.

33. Sharifov, O. F., R. E. Ideker, and V. G. Fast. 2004. High-resolution optical mapping of intramural virtual electrodes in porcine left ventricular wall. *Cardiovasc. Res.* 64:448–456 (see comment).

34. Sharifov, O. F., and V. G. Fast. 2003. Optical mapping of transmural activation induced by electrical shocks in isolated left ventricular wall wedge preparations. *J. Cardiovasc. Electrophysiol.* 14:1215–1222.

35. Ashihara, T., and N. A. Trayanova. 2004. Asymmetry in membrane responses to electric shocks: insights from bidomain simulations. *Biophys. J.* 87:2271–2282.

36. Cheek, E. R., R. E. Ideker, and V. G. Fast. 2000. Nonlinear changes of transmembrane potential during defibrillation shocks: role of Ca^{2+} current. *Circ. Res.* 87:453–459 (See comment.).

37. Maleckar, M. M., M. C. Woods, …, N. A. Trayanova. 2008. Polarity reversal lowers activation time during diastolic field stimulation of the rabbit ventricles: insights into mechanisms. *Am. J. Physiol. Heart Circ. Physiol.* 295:H1626–H1633.

38. Hooks, D. A., K. A. Tomlinson, …, P. J. Hunter. 2002. Cardiac microstructure: implications for electrical propagation and defibrillation in the heart. *Circ. Res.* 91:331–338.

39. Stinstra, J., R. MacLeod, and C. Henriquez. 2010. Incorporating histology into a 3D microscopic computer model of myocardium to study propagation at a cellular level. *Ann. Biomed. Eng.* 38:1399–1414.

40. Roberts, S. F., J. G. Stinstra, and C. S. Henriquez. 2008. Effect of nonuniform interstitial space properties on impulse propagation: a discrete multidomain model. *Biophys. J.* 95:3724–3737.